Catalysis Science & Technology

Accepted Manuscript

ROYAL SOCIETY OF CHEMISTRY

www.rsc.org/catalysis

EFFECT OF Mo/Ce RATIO IN Mo-Ce-Al CATALYSTS ON THE HYDROGEN PRODUCTION BY STEAM REFORMING OF GLYCEROL

GHEORGHIŢA MITRAN[*a], OCTAVIAN DUMITRU PAVEL[a], DANIEL G. MIERITZ[b], DONG-KYUN SEO[b], MIHAELA FLOREA[*a]

[a]Laboratory of Chemical Technology and Catalysis, Department of Organic Chemistry, Biochemistry & Catalysis, Faculty of Chemistry, University of Bucharest, 4-12, Blv. Regina Elisabeta, 030018 Bucharest, Romania

[b]School of Molecular Sciences, Arizona State University, Tempe, AZ, 85287-1604, USA

ABSTRACT

Alumina supported molybdena-ceria catalysts were prepared by sol-gel method and characterized by X-ray diffraction, N_2 sorptometry, UV-VIS-NIR diffuse reflectance spectroscopy, SEM and TEM microscopy. The effect of Mo/Ce ratio, reaction temperature, steam to glycerol molar ratio and space velocity were investigated, as well as the stability of the catalysts during the reaction. The results show that the presence of ceria enhances both the activity and the selectivity toward hydrogen. The best reaction temperature was found to be 500°C for all catalysts, at which the highest hydrogen selectivity of almost 60% was obtained for an optimum cerium loading of 7wt %; higher ceria loading reduced the capacity to convert glycerol into hydrogen.

[*] Corresponding author. E-mail: geta_mitran@yahoo.com ; geta.mitran@chimie.unibuc.ro; mihaela.florea@chimie.unibuc.ro

Keywords: • glycerol steam reforming, • renewable hydrogen, •molybdena-alumina, •ceria-alumina

1. Introduction

In light of concerns related to the environment such as global warming and the exhaustion of fossil fuel a major effort is dedicated to developing and using of alternative energy resources. Either of them is represented by hydrogen because its combustion is free of pollutants [1]. However, hydrogen is not found free in the nature and should be obtained from sources that contain hydrogen. Nowadays, hydrogen production occurs mainly through reforming of fossil fuels [2, 3], but the scope of sustainable development requires the use of alternative sources [4]. For instance at European Union (EU) the level of the energy demand is predicted to be at 20% covered by renewables by 2020 [5]. Therefore, many oxygenated compounds have been used as model for hydrogen production: acetic acid [6], ethylene glycol [7], acetone, glucose [8], phenols [9] and also steam reforming reaction of the aqueous fraction of bio-oil to produce H_2 is very often reported [10].

In the last decade, catalytic reforming of glycerol, obtained as by-product in the biodiesel production process (one ton of glycerol is produced to ten tons of biodiesel), starts to became a conventional method for renewable hydrogen production [11, 12]. Though glycerol is a versatile product which can be used as raw material to produce a variety of chemicals and pharmaceuticals, but also for food and beverages [13, 14], a large excess is still on the market and therefore, is chalenging to find viable processes to obtain products with higher added value from glycerol.

Lately, development of active and stable catalysts at low temperature for glycerol steam reforming is an area of intense research. The CO/H_2 ratio produced by glycerol steam reforming

depends on the reaction conditions and the formulation of the catalyst employed. Different catalytic systems were studied for glycerol reforming, and we found that supported platinum catalysts are the most extensively investigated [15-17], the glycerol conversion being 29% at 250°C, the highest selectivity to reforming (S_{CO2}=45%) and highest yield to H_2 20%, but the high cost of these materials limits their applications. Therefore, many researchers used catalysts less expensive Ni based such as Ni-Cu-Mg [18] that performed high catalytic activity (90% conversion) and 92% hydrogen selectivity at 650°C, Ni-Co [19-21] when the hydrogen fraction reach 77% at 700°C, Mg and Ca incorporated into Ni/SBA-15 [22] the glycerol conversion was 98% and hydrogen yield 53% at 600°C. The disadvantage of these catalysts consists in the facts that are active at high temperatures.

Iriondo et al. studied supported nickel catalysts on modified alumina with Ce, Mg, Zr and La to produce hydrogen from glycerol [23] and they found that the selctivity to hydrogen and stability of nickel phases increases for Ce and La containing samples.

Numerous studies have shown that a combination of two metal oxides on support provides better activity, due to the positive effects derived from the interactions between the two metals, and therefore we decided to investigate the steam reforming of glycerol on molybdena-ceria based catalysts. Ceria is one of the most studied catalysts; an important property being its reductibility, characterized by the relatively facile change in oxidation state from Ce^{+4} to Ce^{+3} by formation of oxygen vacancies or by addition of electrons [24], while molybdenum is one main component of the catalysts for the selective oxidation, as for example methane [25], propene [26], etc.

The literature survey shown that molybdena-ceria on alumina were good catalysts for water gas shift reaction [27], methanation [28], oxidation [29, 30] or, esterification [31], but no results on glycerol steam reforming on these materials were yet reported.

In the present paper, we report results obtained in glycerol steam reforming over Mo-Ce/Al_2O_3 catalysts. Various techniques including N_2 adsorption-desorption, X-ray diffraction (XRD), transmission electron microscopy (TEM), scanning electron microscopy (SEM), UV-vis spectroscopy were performed to characterize the prepared catalysts. The effect of Mo/Ce ratio, reaction temperature, steam to glycerol molar ratio, space velocity and the catalysts stability were investigated.

2. **Experimental**

2.1. Catalysts preparation

Alumina supported molybdena-ceria catalysts were prepared by a combined sol-gel and gel combustion method. The reported method consists of gelling and further combustion of an aqueous solution of salts which contains desired metals and fuel, giving a product with large surface area.

Aluminum nitrate ($Al(NO_3)_3$•9 H_2O from Tunic) was dissolved in distilled water and the solution (10% concentration) was stirred at 60°C for 30 min. Citric acid ($C_6H_8O_7$•H_2O, from Silal, 99.5% purity) was added in the solution, with a molar ratio citrate-to-nitrate of 0.5. Then aqueous $(NH_4)_6Mo_7O_{24}$•$4H_2O$ (Fluka Analytical) and $Ce(NO_3)_3$•$6H_2O$ (from Aldrich) solutions were added, so as to get a weight percentage of 10% Mo and 3, 7 and 10% Ce on alumina. The excess of water was slowly evaporated at 80°C to obtain a gel. The gel was rapidly heated at 200°C. Finally, all the prepared materials were calcined in flowing air at 400°C for 2 h and

subsequently at 550°C for 2 h. The catalysts were denoted as function of Ce percentage deposited on alumina: MoAl, MoCe3Al, MoCe7Al and MoCe10Al.

2.2. Catalysts characterization

Powder X-ray diffraction (PXRD) patterns were obtained with a Philips PW3710 diffractometer equipped with a Cu K_α source (λ = 1.5405 Å), operating at 50 kV and 40 mA. They were recorded over the 5–80° angular range with 0.02° (2θ) steps and an acquisition time of 1 s per point. Data collection and evaluation were performed with PC-APD 3.6 and PC-Identify 1.0 software.

The surface areas of the catalysts were measured from the adsorption isotherms of nitrogen at −196°C using the BET method with a Micromeritics ASAP 2020 sorptometer. The samples were first out-gassed at 300°C for 4 h in the degas port of the adsorption apparatus. The Barrett–Joyner–Halenda (BJH) method was applied to the desorption branch to calculate the pore size distribution, using the Halsey thickness curve, heterogeneous surface and Faas correction for multilayer desorption. The total pore volume is obtained by applying relative pressure (P/P_0) between 0.004 and 1.

Scanning electron microscopy (SEM) studies were performed on lightly-crushed samples deposited carbon tape by using an FEI XL-30 Environmental SEM with 5-15 keV electrons. Before analysis, using a Denton Desk II sputter-coater, the samples were coated with an Au-Pd (60-40) target for 140 s to deposit a coating of ~ 12 nm.

For transmission electron microscopy (TEM) studies, samples were prepared by dry-grinding and dusting on to TEM grids. The images were collected on a JEOL 2010F at an accelerating voltage of 200 kV.

The UV-VIS-NIR spectra were recorded using UV3600 UV-VIS spectrophotometer with Shimadzu ISR-3100 integrating sphere attachment having angle of incident light 0-8°, wavelength range 220-2600 nm, two light sources: D_2 (deuterium) lamp for the ultraviolet range and WI (halogen) lamp for the visible and near-infrared range. UV-VIS-NIR spectrophotometer has three detectors, consisting of a PMT (photomultiplier tube) for the ultraviolet and visible regions and InGaAs and cooled PbS detector for the near-infrared region. The spectra were recorded in the range of 220-800 nm (the switching wavelength of the lamps is between 282 nm and 393 nm) with a wavelength step of 2 nm, having the slit width of 8 nm. The UV-VIS spectra were measured using samples diluted with extra pure barium sulfate (purchased from Nacalai Tesque).

2.3. Catalytic tests

Glycerol steam reforming experiments were carried out in a fixed-bed quartz reactor (12 mm internal diameter) at atmospheric pressure over 0.1 g of catalyst. A water/glycerol solution (with water to glycerol molar ratio 9:1, 15:1 and 20:1) was fed into the reactor by a pump (Verder peristaltic 2000) with a space velocity between 6.4 - 12.9 g gly/g cat·h and with N_2 as carrier gas (30 ml/min). The reaction was performed at different temperatures between 400-500°C; the evaporation was carried out in the first third of the reactor. The reaction products were analyzed (every 30 min) with a Thermo Finnigan Gas-Chromatograph equipped with a thermal conductivity detector (TCD) with an alumina column and GC K072320 Thermo-Quest chromatograph equipped with FID detector.

The glycerol conversion in gaseous products is expressed as:

$$X_g\,(\%) = \frac{N_{CO2}+N_{CO}+N_{CH4}}{3*N_{C3H8O3in}} \cdot 100$$

and the gaseous products selectivity is expressed as:

$$S_i\ (\%) = \frac{N_i}{N_{H2}+N_{CO2}+N_{CO}+N_{CH4}} \cdot 100$$

where N_{H2}, N_{CO2}, N_{CO} correspond to produced moles of H_2, CO_2, CH_4, CO

3. Results and discussion

3.1. Catalysts characterization

The PXRD patterns for alumina supported molybdena-ceria catalysts are shown in Figure 1.

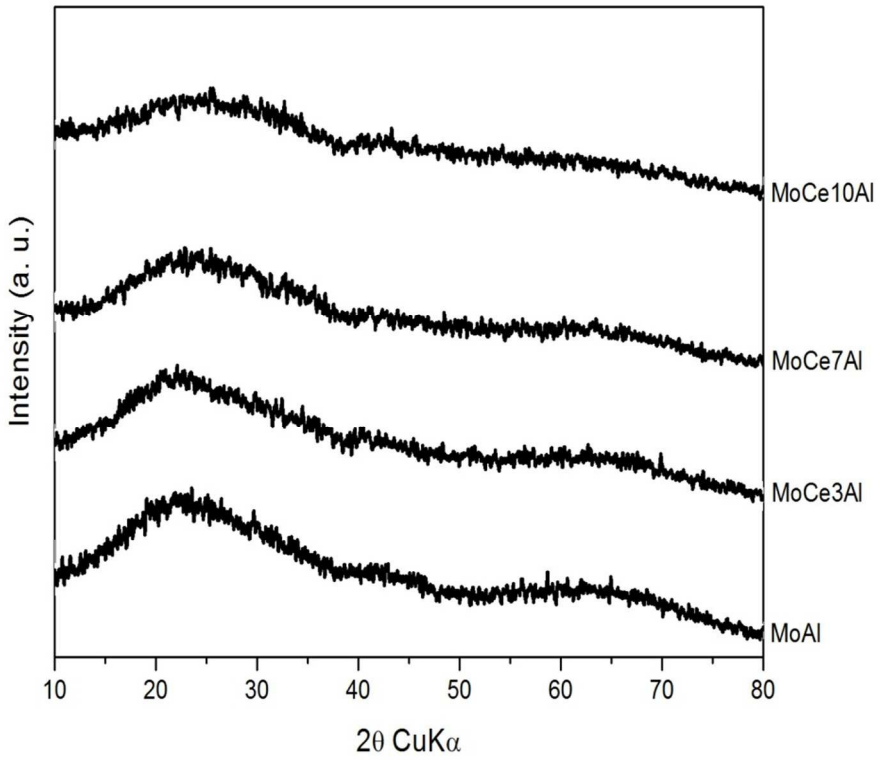

Fig. 1. XRD patterns of alumina supported molybdena-ceria catalysts

The samples exhibit a broad peak at 2θ ~ 20-30° corresponding to amorphous phase of alumina, which is in agreement with previous reports from the similar synthetic processes [32, 33]. No traces of MoO_3 or CeO_2 phases were detected, suggesting that molybdena and ceria are well dispersed with the amorphous alumina.

The textural and structural characteristics are shown in Table 1, which also reports amounts of molybdena and ceria on alumina support as determined by SEM-EDX analysis.

Table 1. Physico-chemical characteristics of the catalysts.

Catalyst	Specific surface area (m^2/g)	Total pore volume (cc/g)	Average pore width (nm)	Average pore diameter (nm)	Chemical composition (wt%) by EDX[a]			Chemical composition (at%) by EDX[a]		
					Mo	Al	Ce	Mo	Al	Ce
MoAl	195.4	0.20	4.7	4.1	9.7	61.2	0	2.4	54.1	0
MoCe3Al	219.2	0.13	2.4	2.7	7.7	47.9	3.3	1.8	39.9	0.5
MoCe7Al	190.5	0.14	3.2	3.2	6.3	39.0	6.9	1.5	31.8	1.1
MoCe10Al	178.8	0.11	2.2	2.7	7.3	40.6	9.1	1.8	34.7	1.5

[a-] Oxygen in balance

While the Mo content is consistent with the 10% nominal loading for MoAl, the elemental analysis showed a Mo content between 6.3 and 7.7 % for the Ce-containing catalysts. The catalysts showed high surface area (> 170 m^2/g), and the samples containing ceria showed a decreased surface area with an increase in cerium content. The nitrogen isotherms (Figure 2a) show a small hysteresis loop indicating the presence of mesopores. The catalysts show type IV isotherms and over $P/P_o = 0.5$ samples with ceria adsorb a lower volume of nitrogen compared to sample without ceria. The total pore volumes and average pore diameters are diminished upon addition of ceria; from 0.20 to 0.11 cm^3/g and from 4.1 to 2.7 nm respectively, suggesting that the presence of ceria could cause pore closure or pore shrinkage. All samples present small mesopores (pore diameters 2-10 nm) and the sample with molybdena presents a higher mesoporosity compared to molybdena-ceria samples (Figure 2b).

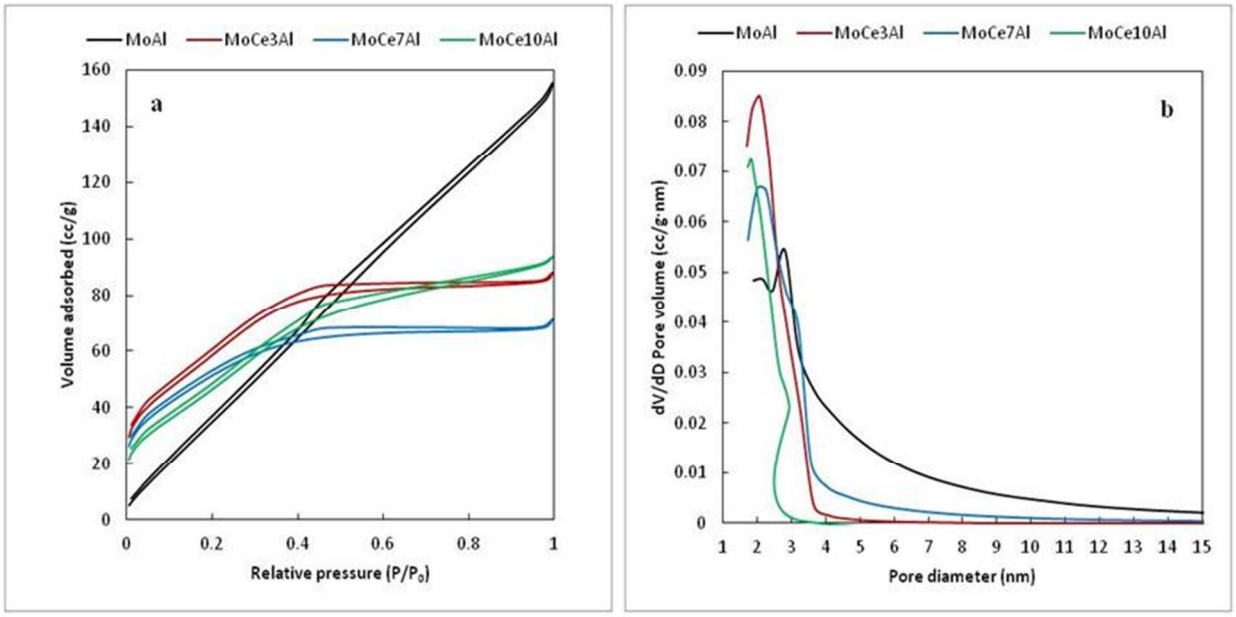

Fig. 2. Nitrogen adsorption–desorption isotherms (a) and BJH pore size distribution (b) of MoCeAl samples

The results of surface area are in good agreement with the observations from XRD patterns indicating a very good dispersion of molybdena and ceria on the support. The fact that the decrease of the specific surface area is not so important as compared to the one of alumina (232 m^2/g), confirms the good dispersion of cerium and molybdenum on our support.

The EDX analysis confirmed the percentage of Mo and Ce deposited on alumina during the preparation (Table 1), suggesting that the sol-gel method used for the preparation of these materials is an efficient one.

In Figure 3 the SEM images of the samples MoAl (a), MoCe3Al (b), MoCe7Al (c) and MoCe10Al (d) reveal that all the alumina-based catalyst particles exhibit similar morphological characteristics with irregular shapes and sizes in the range of microns.

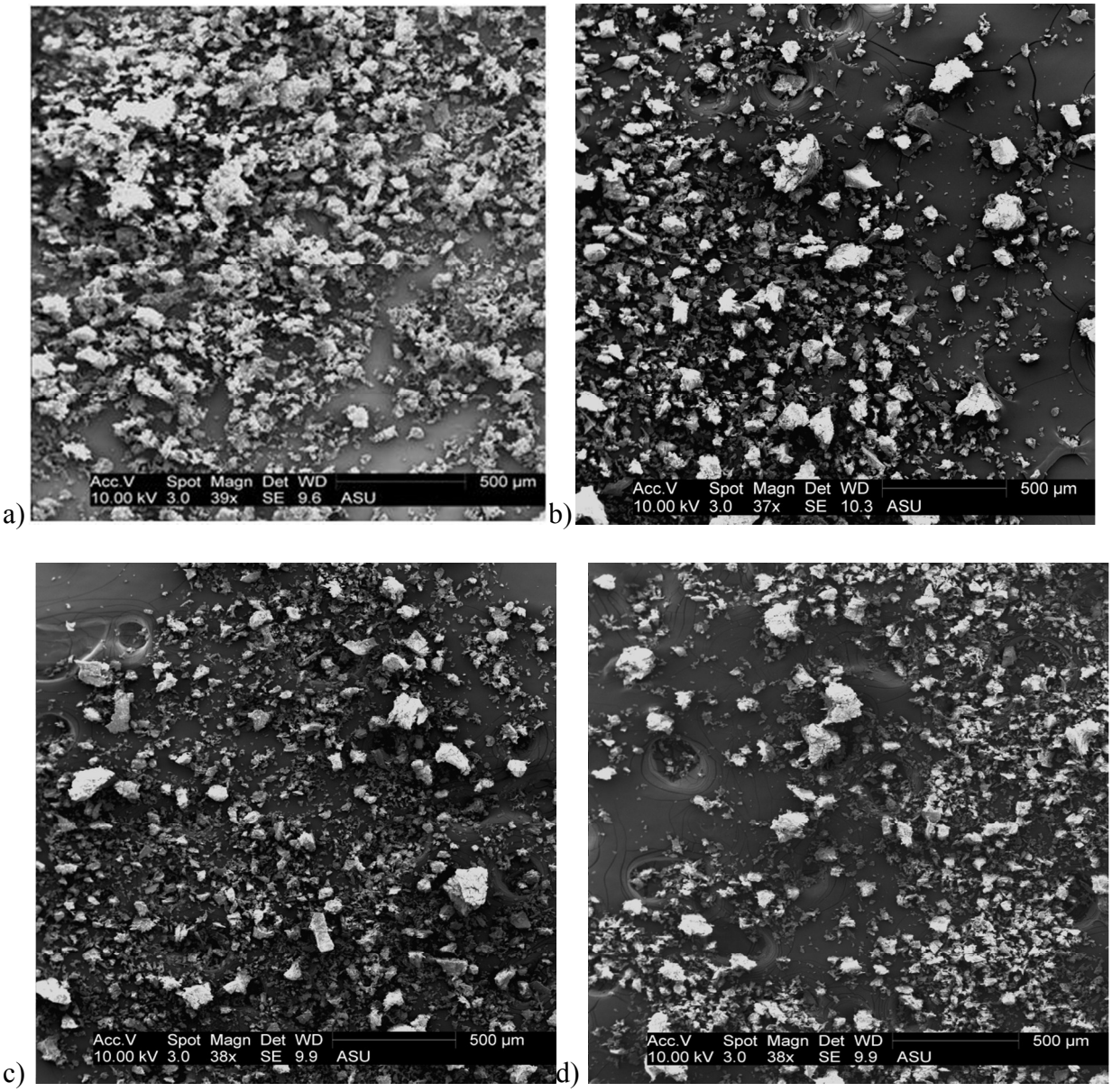

Fig. 3. SEM images of MoAl (a), MoCe3Al (b), MoCe7Al (c) and MoCe10Al (d) catalysts. Scale bar = 500 µm.

The TEM micrographs in Figure 4 are shown for the same respective samples as for SEM in Figure 3. Two frames are shown for each sample with scale bars of 100 and 500 nm. Images at the lower magnification on the rights show individual shards of the catalysts, and the contrast suggests that they are relatively thick in the middle and become thin at the edges. At the higher

magnification, all the samples show small pores (~ 2 nm) that are evenly dispersed throughout the surface giving them a sponge-like appearance. Due to the thickness of the particles, discernable pore size measurement was not possible, although the observed pores are in agreement with the results from BJH analysis.

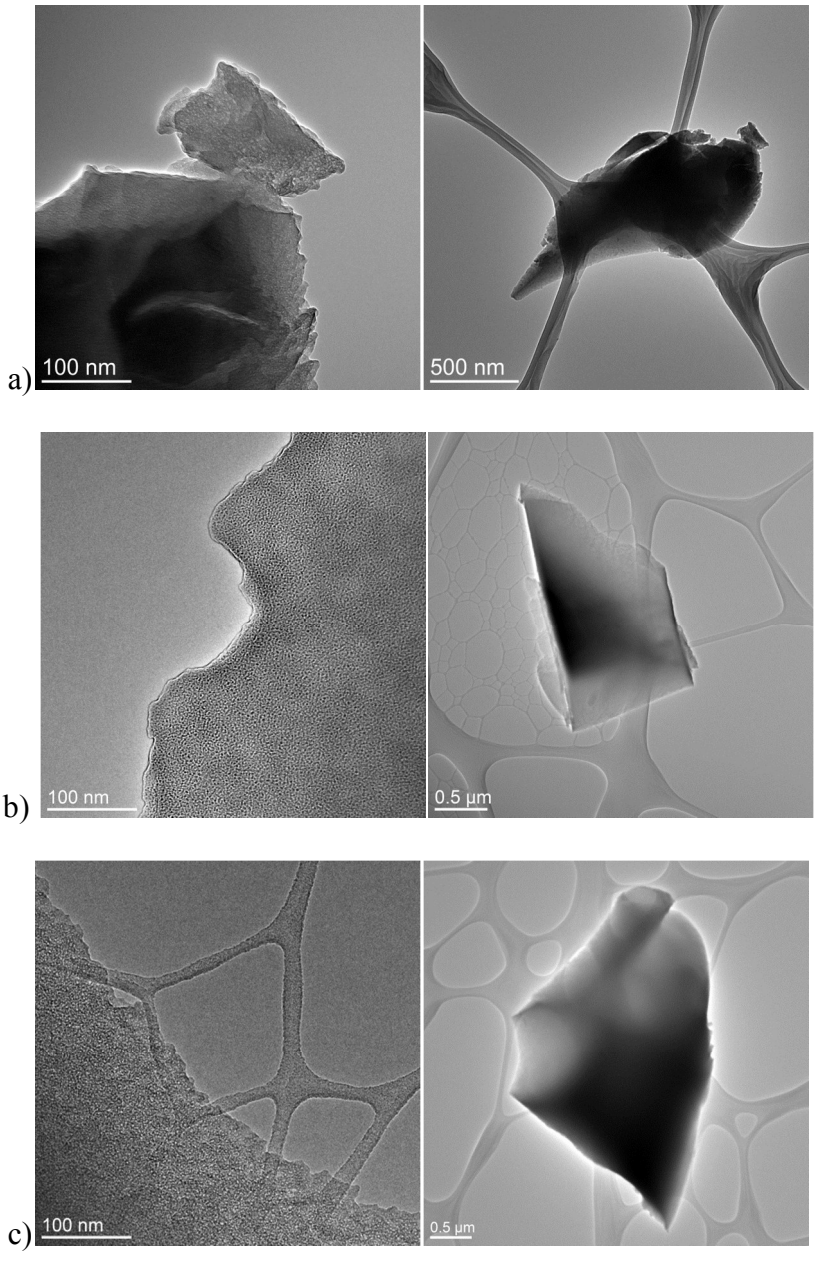

d) 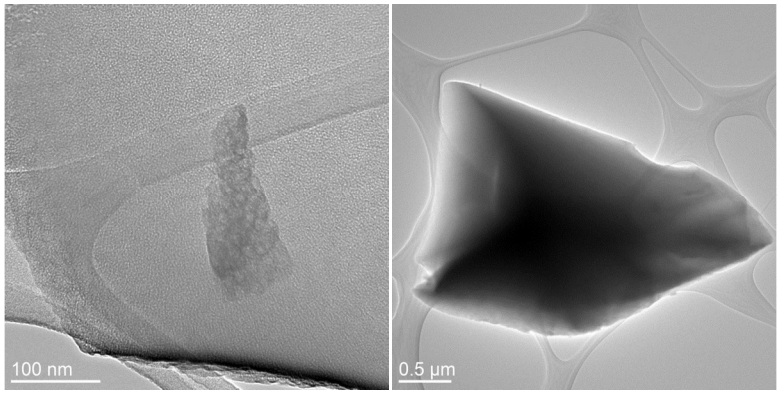

Fig. 4. TEM micrographs of MoAl (a), MoCe3Al (b), MoCe7Al (c) and MoCe10Al (d) catalysts.

Scale bar = 100 nm (left) and 500 nm (right).

The UV-VIS spectra for all studied catalysts are shown in Figure 5.

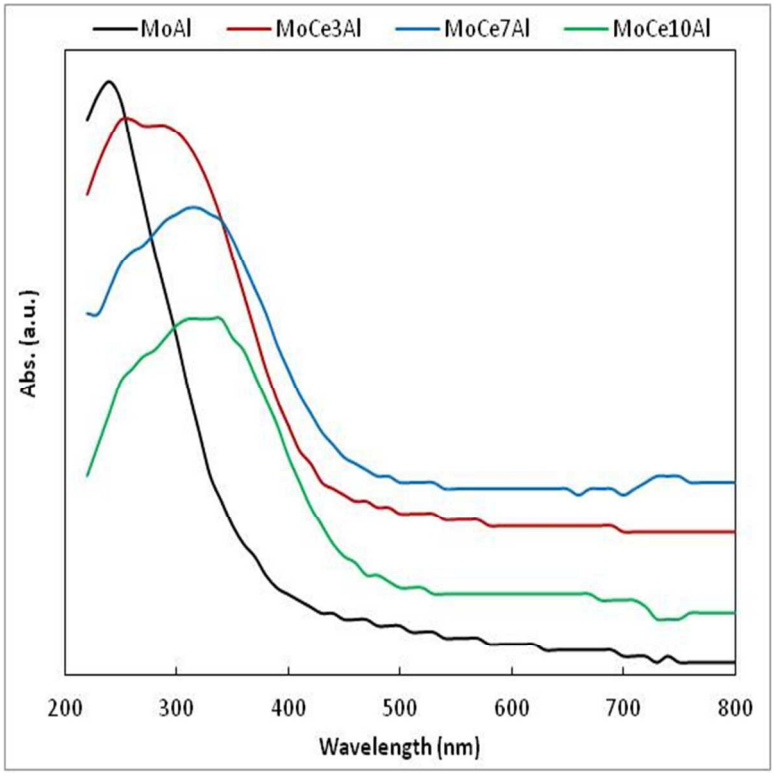

Fig. 5. UV-VIS spectra of MoAl and MoCeAl catalysts

In the literature, the bands at 210-250 and 300-335 nm are due to charge transfer transitions from p orbitals of oxygen to d orbitals of molybdenum ($O^{2-} \rightarrow Mo^{6+}$) in monomeric tetrahedral and polymeric octahedral Mo-oxo species [34, 35]. $O^{2-} \rightarrow Ce^{4+}$ (from p orbitals of oxygen to f orbitals of cerium) charge transfer bands are centered at about 280 nm and inter-band transitions are located at 340 nm [36, 37]. Among our samples, MoAl exhibits a band at 240 nm, while MoCe3Al shows two bands at 260 and 290 nm, MoCe7Al and MoCe10Al have four bands located at 260 (250), 290 (280), 320 (310) and 340 (340) nm.

For all the samples with ceria, the band corresponding to tetrahedral coordination of molybdenum is shifted to longer wavelengths from 240 to 260 nm. The 240 nm band of the catalyst MoAl indicates the presence of only tetrahedral molybdenum species, as indicated in the previous report for the low Mo loading [38, 39]. The red shift of the absorption band for the Ce-containing samples may be due to the presence of ceria that induces the change in molybdenum coordination, to octahedral. For MoCe7Al the intensity of the band at 320 nm corresponding to octahedral molybdena is more intense compared with the band at 340 nm from ceria, while for MoCe10Al those two bands have the same intensity.

In a tetrahedral Mo system like $(MoO_4)^{2-}$(monomers), $(Mo_2O_7)^{2-}$ (dimers) or $(Mo_3O_{10})^{2-}$ (trimers) have a higher negative charge density in comparison to octahedral Mo species (MoO_3 or $[Mo_7O_{24}]^{6-}$) [40]. Since alumina support has a positively charged surface, the more negatively charged tetrahedral Mo species are stabilized preferably on this support. Incorporation of ceria in the catalyst led to a weaker interaction between the alumina support and the molybdate clusters, as observed for the catalysts with ceria wherein Mo is octahedrally coordinated. It is also worth mentioning the presence of two different ceria species: dispersed and bulk. The first are most probably Ce^{3+}-like species and the second are bulk CeO_2 crystallites with size less than 4 nm that

are not detectable by XRD [41]. In any event, the existence of synergetic interaction between Ce and Mo is evidenced from UV-VIS spectroscopy by splitting and shifting of the bands in the range of 250-350 nm. This interaction might occur between the molybdate monolayer and the Ce incorporated in the molybdate monolayer or possibly in bilayer.

3.2. Steam reforming of glycerol

This research has as main objective to study the effect of operating conditions over Mo-Ce-Al catalysts. The experiments were carried out by varying the following parameters: temperature, glycerol to steam molar ratio and space velocity. Glycerol steam reforming for hydrogen production is following the reaction (eq 1):

$$C_3H_8O_3 + 3H_2O = 3CO_2 + 7H_2 \qquad \Delta H^0 = +123 \text{ kJ/mol} \qquad (1)$$

which is the result of the combination of glycerol decomposition (eq 2) and Water Gas Shift reaction (eq 3)

$$C_3H_8O_3 = 3CO + 4H_2 \qquad \Delta H^0 = +245 \text{ kJ/mol} \qquad (2)$$

$$CO + H_2O = CO_2 + H_2 \qquad \Delta H^0 = -41 \text{ kJ/mol} \qquad (3)$$

It was demonstrate by DFT calculation [42] that the catalyst must promote the cleavage of C-C, O-H, and C-H bonds in steam reforming reaction, in order to favor H_2 production and CO, and facilitate the water gas shift reaction to remove adsorbed CO from the surface as CO_2 (eq 3), conversely to the cleavage of C-O bonds leading to alkanes.

From termodinamic studies on steam reforming of glycerol [43] it was concluded that optimal conditions for hydrogen production were a temperature of 650 - 700°C and a water/glycerol ratio of 9-12 at atmospheric pressure. Unfortunately, glycerol has low thermal stability and associated with its high oxygen content it is very difficult to perform the reaction at such a high temperature because high reaction temperatures lead to the formation of a variety of

products and severe coking of catalyst. Therefore, reforming the glycerol at lower temperatures is an important challenge for this study, and the influence of the reaction temperature over the catalytic activity was evaluated further.

The effect of temperature on glycerol steam reforming is illustrated in Figure 6 for all prepared samples at a steam to glycerol molar ratio of 15:1.

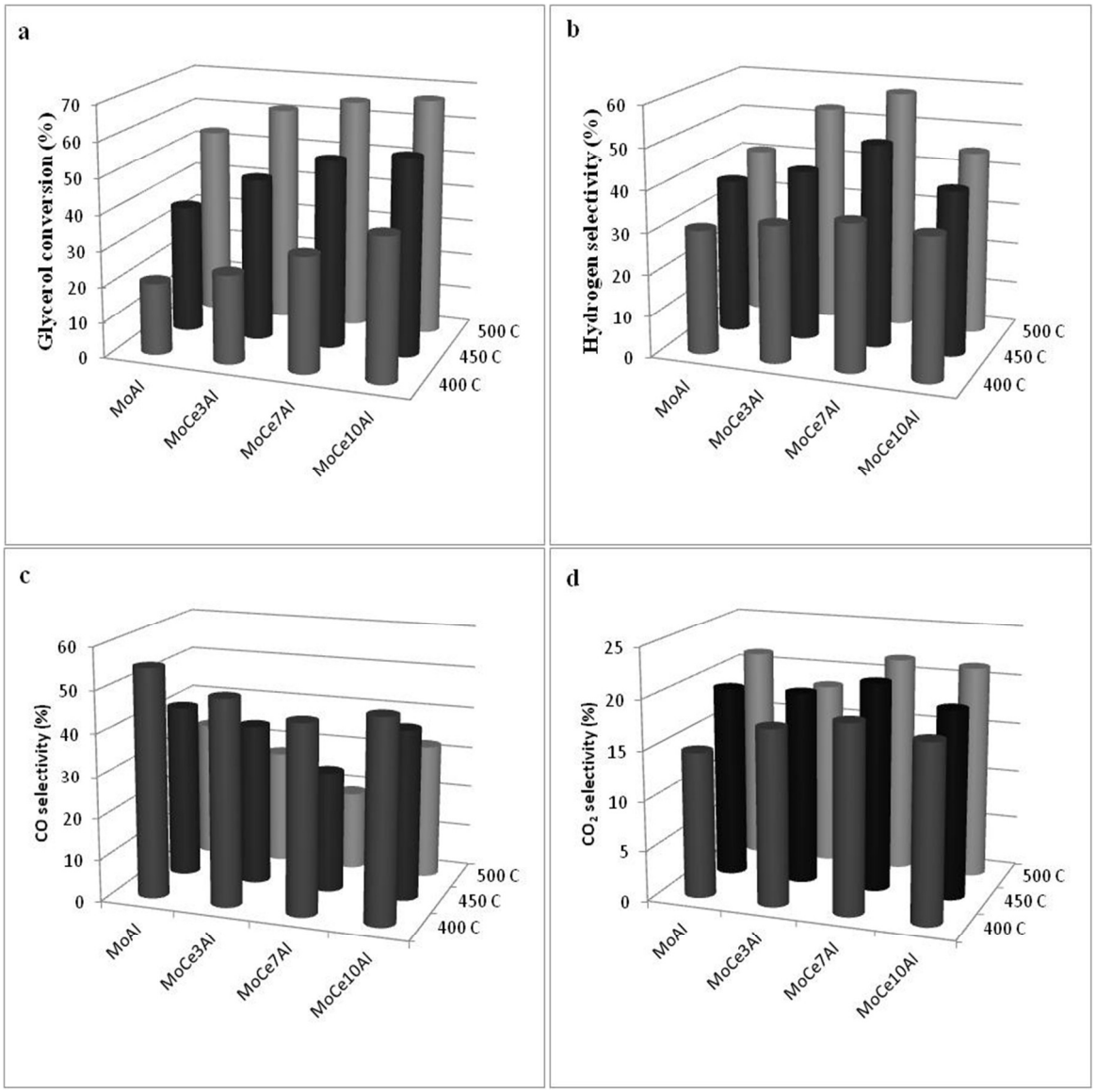

Fig. 6. Effect of temperature during the steam reforming of glycerol on MoCeAl catalysts: glycerol conversion (a), H_2 (b), CO (c) and CO_2 (d) selectivity (reaction conditions: steam to glycerol molar ratio 15:1, space velocity 9.2 g gly/g cat·h)

The main gas products obtained are H_2, CO, CO_2 but were also observed small amounts of CH_4. Methane formation may proceed from methanation reaction of CO or CO_2 with H_2 (eq 4 and eq 5)

$$CO + 3H_2 = CH_4 + H_2O \qquad \Delta H^0 = -206 \text{ kJ/mol} \qquad (4)$$

$$CO_2 + 4H_2 = CH_4 + 2H_2O \qquad \Delta H^0 = -165 \text{ kJ/mol} \qquad (5)$$

For all temperatures studied, the activity increases when ceria is added and is directly proportional with ceria content (Fig. 6a). Concerning the selectivity to the reaction products as a function of the reaction temperature, no matter the catalyst studied, the following trends were observed: i) the hydrogen selectivity increased (Fig. 6b), while CO selectivity decreased (Fig. 6c) with the temperature increasing from 400 to 500°C; ii) the CO_2 selectivity reaches a maximum at 500°C (Fig. 6d); iii) the molar ratio H_2/CO increases and molar ratio CO/CO_2 decreases with temperature increasing.

The global reaction of glycerol reforming can be also described as:

$$C_3H_8O_3 + xH_2O \rightarrow (3\text{-}x)CO + xCO_2 + (4+x)H_2 \qquad (6)$$

The reaction shifts to glycerol pyrolysis when x=0, to glycerol reforming when x=3 and to syngas production between the two stoichiometries of x [44]. In case of our catalysts, from the data presented in Figure 6, x=0.6-1.2 for MoAl and x=2.4-2.9 for catalysts with ceria suggesting that these materials are more selective in glycerol steam reforming and syngas production. The best reaction temperature was found to be 500°C for all catalysts, at which the highest hydrogen selectivity of almost 60% was obtained for an optimum cerium loading of 7wt %, for MoCe7Al

sample; higher ceria loading reduced the capacity to convert glycerol into hydrogen. These results are in agreement with one obtained by Iriondo et al. [23] which investigated the effect of ceria promotion over Ni/Al_2O_3 and showed that the incorporation of low ceria loadings enhanced the catalytic activity but the increase of ceria amounts reduced the selectivity to hydrogen. The literature survey shown that Dave et al [45] have studied $Ni\text{-}Zr/CeO_2$ catalysts and obtained conversion between 37-68% and hydrogen selectivity 73-78% at 600°C. Also, in our previous work [46] was studied glycerol steam reforming over molybdena supported on alumina and the hydrogen selectivity was between 52-68% at a conversion of 40-58% at 500°C. Adhikari [47] achieved a conversion of 94% and hydrogen selectivity of 70% on $Rh/CeO_2/Al_2O_3$ catalyst at 900°C. Therefore, the results of the present study indicate that Mo-Ce oxide catalysts are very promising for glycerol reforming reaction.

Useful information can be obtained from the values of the H_2/CO_2 and H_2/CO ratios. Therefore, MoAl catalyst has a H_2/CO_2 ratio at 400°C very closely to theoretical ratio of 2.33 (our result is 2.1), while at 500°C H_2/CO ratio is close to theoretical ratio of 1.33 (our result is 1.24). These results suggest that on MoAl sample at low temperature, steam reforming and water gas shift reaction are favoured reactions and at higher temperature decomposition of glycerol into syngas is favoured [41]. For the samples containing ceria the results are different: MoCe3Al catalyst has a H_2/CO_2 ratio of 2.1 and H_2/CO ratio of 1.1 at 450°C; MoCe7Al catalyst has a H_2/CO_2 ratio of 2.35 and H_2/CO ratio of 1.7 at 450°C while MoCe10Al catalyst has a H_2/CO_2 ratio of 2.1 and H_2/CO ratio of 1.4 at 500°C suggesting that on these catalysts all reactions occur simultaneously. To summarize, at 500°C, the presence of Ce in the catalyst promotes the water-gas-shift reaction increasing the H_2 production and decreasing the selectivity of CO, with an optimum for MoCe7Al sample. According with the literature data [48], the role of CeO_2 is to

activate H_2O and to provide the required oxygen for the oxidation of glycerol. The addition of ceria improved the ability to store, release, and transfer oxygen species of the catalyst, resulting in an enhanced catalytic activity.

In Figure 7 are depicted the glycerol conversion and selectivity to H_2 as a function of Mo and Ce surface density, as calculated from EDX analysis. The surface density of molybdenum and cerium, defined as the number of metal atoms present per specific surface area unit, is expressed by the following equation:

$$\text{Surface density } (M_{atoms}/nm^2) = \frac{wt\%\ Molybdenum/Cerium\ loading \cdot 6.023 \cdot 10^{23}}{Molecular\ Weight\ of\ Molybdenum/Cerium \cdot 100 \cdot Surface\ Area}$$

It was found that a higher glycerol conversion is related to ceria content, increasing with the cerium surface density. Conversely, for the hydrogen selectivity it exist an optimum cerium distribution which corresponds to a cerium loading of 7%; for this sample molybdenum surface density has the lowest value. Higher amount of cerium determine the decreases of the hydrogen selectivity due probably to a higher tendency of ceria to interact with alumina and/or molybdena [49]. Synthesizing, the hydrogen selectivity can be attributed to the kind of molybdena species and to their surface densities, more octahedral molybdena species and lower density on the surface leading to higher selectivity.

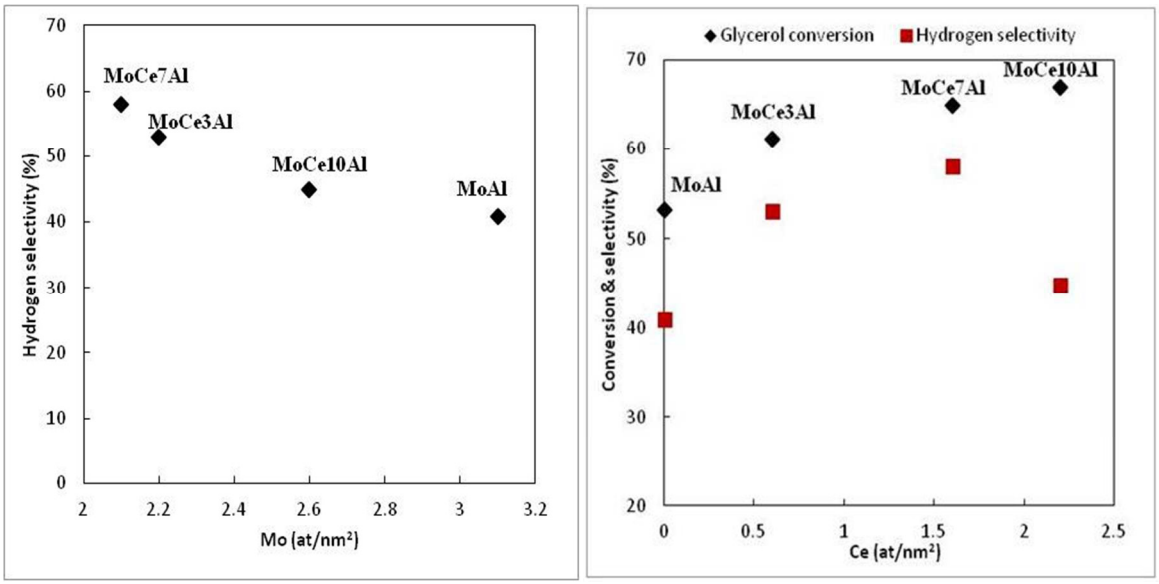

Fig. 7. Correlation between Mo and Ce surface density, and hydrogen selectivity, glycerol conversion (reaction conditions: 500°C, steam to glycerol molar ratio 15:1, space velocity 9.2 g gly/g cat·h)

As mentioned previously, the steam to glycerol molar ratio plays an important role on the efficiency to H_2 production. Therefore, we studied the effect of steam to glycerol molar ratio (between 9:1 and 20:1) for all prepared samples on glycerol conversion and products selectivities at 500°C, and the results are presented in Figure 8. For all tested samples, glycerol conversion (Fig. 8a) increased significantly by decreasing glycerol concentration in the feed. The highest value of almost 85% is obtained for MoCe7Al for a steam to glycerol ratio of 20:1.

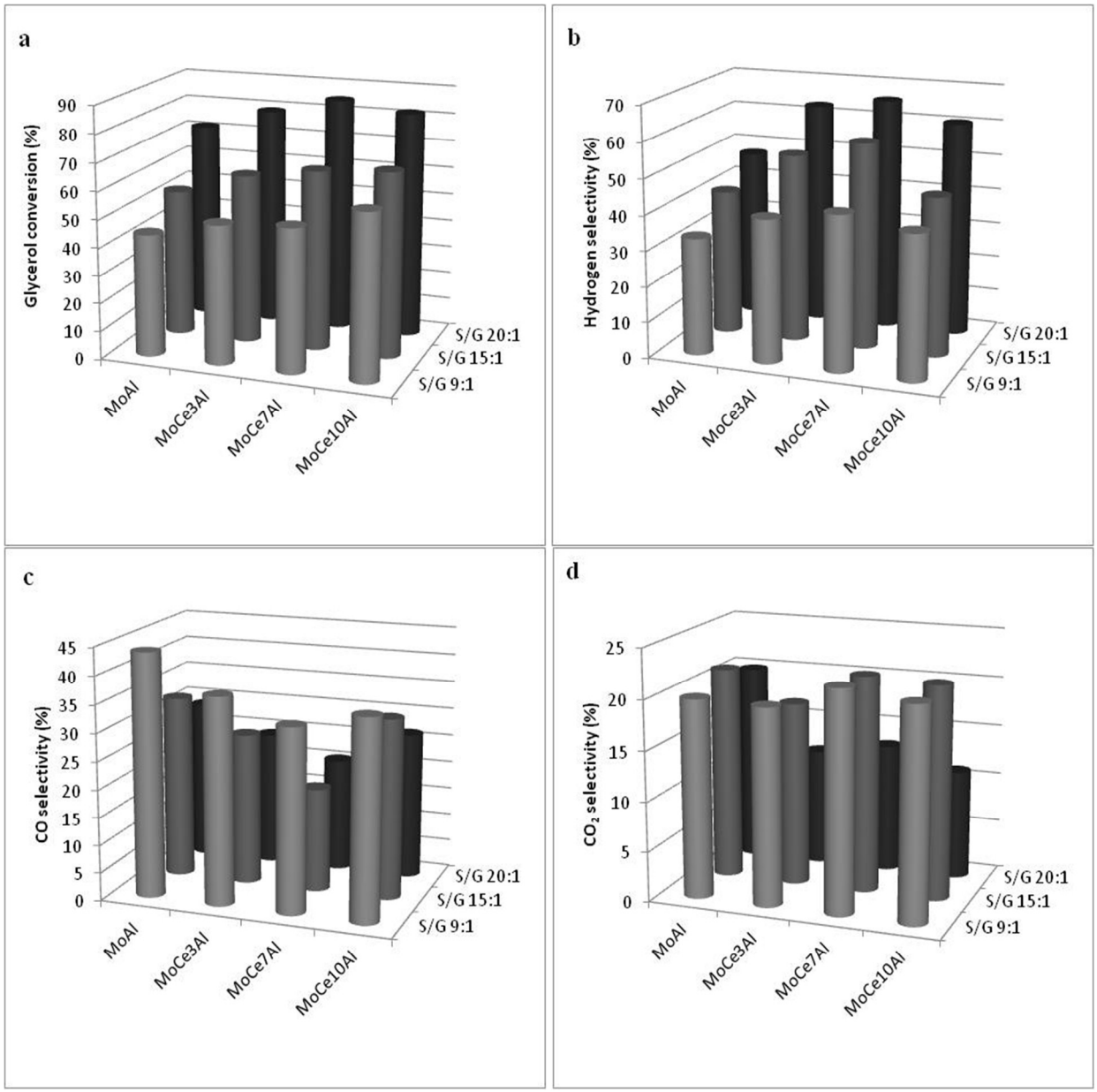

Fig. 8. Effect of steam/glycerol molar ratio during the steam reforming of glycerol on MoCeAl catalysts: glycerol conversion (a), H_2 (b), CO (c) and CO_2 (d) selectivity (reaction conditions: 500°C, space velocity 9.2 g gly/g cat·h)

The hydrogen selectivity (Fig. 8b) increased also significantly by decreasing the glycerol concentration in the feed, while CO (Fig. 8c) and CO_2 (Fig. 8d) selectivities decreased

accordingly. Thus, it is obvious that high water content in the feed facilitates H_2 production, but it is worthy of note that a higher water-to-glycerol ratio in the feed will result in higher energy requirement for the evaporation of higher amounts of water. Therefore, the experiments performed in this study were done at lower steam to glycerol ratio.

The glycerol conversion and selectivity at different space velocity (6.4, 9.2 and 12.9 g gly/g cat·h) on MoCe7Al catalyst are shown in Figure 9.

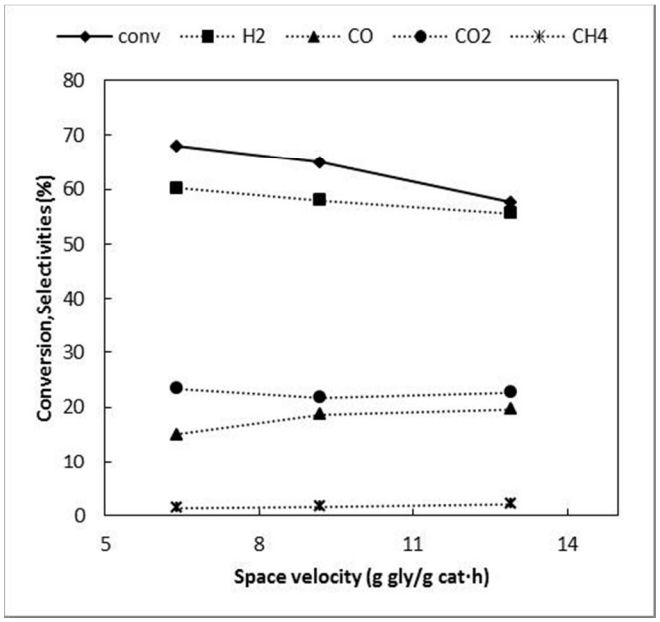

Fig. 9. Influence of space velocity on glycerol conversion and hydrogen selectivity over MoCe7Al catalyst (reaction conditions: 500°C, steam to glycerol molar ratio 15:1)

Conversion and hydrogen selectivity decrease slightly with the increase of the space velocity. The results suggest that, at lower space velocity the steam reforming into H_2 and CO_2 is favored. By increasing the space velocity, the amount of CO increased slightly as well as CH_4 selectivity, indicating the occurrence of the glycerol decomposition (eq 2), together with the CO_2 methanation (eq 5) in this reaction conditions.

The catalyst stability in a catalytic process represents an important goal to be taking into account, in order to assess the practical use for the new catalytic systems. Therefore, the stability was evaluated for glycerol steam reforming at 500°C on MoCe7Al sample, this being the most selective and the results are shown in Figure 10.

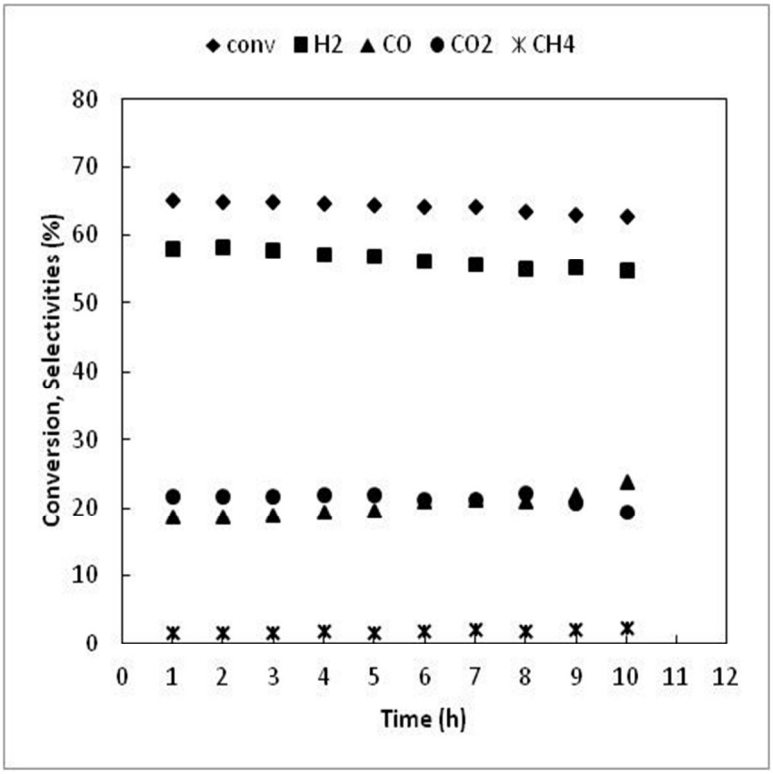

Fig.10. Stability test for 10 h on stream over MoCe7Al catalyst (reaction conditions: 500°C, steam to glycerol molar ratio 15:1, space velocity 9.2 g gly/g cat·h)

The conversion and the selectivity of H_2 decrease only very slowly during the 10 h of stream, suggesting that our catalytic system present a good stability for at least 10 h of time on stream.

Conclusion

Molybdena-ceria supported on alumina is a promising catalyst in steam reforming of glycerol an interesting way to achieve environmentally friendly hydrogen. The catalytic activity of the studied samples indicated clearly the important catalyst properties necessary to carry out steam reforming of glycerol: i) it was found that a higher activity to glycerol steam reforming is related to ceria content and a higher selectivity to hydrogen with a lower molybdena density on the surface; ii) the molybdena-alumina catalyst has only tetrahedral molybdena species on the surface while upon ceria addition the presence of octahedral species of molybdenum was evidenced, contributing to increasing both activity and hydrogen selectivity.

Acknowledgements

This work was supported by a grant of the Romanian National Authority for Scientific Research, CNDI–UEFISCDI, project number PCCA-II-56/2014.

References

[1] A.A. Lemonidou, P. Kechagiopoulos, E. Heracleous, S. Voutetakis, *The Role of Catalysis for the Sustainable Production of Bio-fuels and Bio-chemicals*, (2013) 467-493

[2] K. Liu, C. Song, V. Subramani, Hoboken, New Jersey, USA: *AIChE-Wiley, John Wiley & Sons Inc* (2010)

[3] B.C.R. Ewan, R.W.K. Allen, *Int. J. Hydrogen Energy* 30 (2005) 809-819

[4] A. Tanksale, J.N. Beltramini, G.M. Lu, *Renew. Sustain. Energ. Rev*. 14 (2010) 166-182

[5] European Commission Energy roadmap 2050. COM (2011) 885/2, Brussels, Belgium

[6] E.C. Vagia, A.A. Lemonidou *J. Catal.* 269 (2) (2010) 388-396

[7] C. Wu, R. Liu, *Int. J. Hydrogen Energy* 36 (4) (2011) 2860-2868

[8] X. Hu, G. Lu, *Appl. Catal. B. Environ*. 88 (2009) 376-385

[9] K. Polychronopoulou, C.N. Costa, A.M. Efstathiou, *Catal. Today* 112 (1-4) (2006) 89-93

[10] R. Trane, S. Dahl, M.S. Skjøth-Rasmussen, A.D. Jensen, *Int. J. Hydrogen Energy* 37 (2012) 6447-6472

[11] M. Slinn, K. Kendall, C. Mallon, J. Andrews, *Bioresour. Technol*. 99 (2008) 5851–5858

[12] A. Gallo, C. Pirovano, P. Ferrini, M. Marelli, R. Psaro, S. Santangelo, G. Faggio, V. Dal Santo, *Appl. Catal. B: Env*. 121– 122 (2012) 40– 49

[13] M. Pagliaro, R. Ciriminna, H. Kimura, M. Rossi, C.D. Pina, *Angew Chem. Int*. Ed. 46 (2007) 4434-4440

[14] D.T. Johnson, K.A. Taconi, *Environ. Progr*. 26(4) (2007) 338-348

[15] B. Meryemoglu, B. Kaya, S. Irmak, A. Hesenov, O. Erbatur, *Fuel* 97 (2012) 241-244

[16] D.Ö. Özgür, B.Z. Uysal, *Biomass Bioenergy* 35 (2011) 822-826

[17] M.L. Barbelli, F. Pompeo, G.F. Santori, N.N. Nichio, *Catal. Today* 213 (2013) 58-64

[18] C. Wang, B. Dou, H. Chen, Y. Song, Y. Xu, X. Du, L. Zhang, T. Luo, C. Tan, *Int. J. Hydrogen Energy* 38 (2013) 3562 -3571

[19] Esteban A. Sanchez, Rau´l A. Comelli, *Int. J. Hydrogen Energy* 39 (2014) 8650 -8655

[20] C.K. Cheng S.Y. Foo, A.A. Adesina, *Catal. Today* 164 (2011) 268-274

[21] C.K. Cheng S.Y. Foo, A.A. Adesina, *Ind. Eng. Chem. Research* 49 (2010) 10804-10817

[22] J.A. Calles, A. Carrero, A.J. Vizcaíno, L. García-Moreno, *Catal. Today* 227 (2014) 198–206

[23] A. Iriondo, V.L. Barrio, J.F. Cambra, P.L. Arias, M.B. Guemez, R.M. Navarro, *Top. Catal*. 49 (2008) 46-58

[24] M. Nolan, *Catalysis by Materials with Well-Defined Structures*, (2015) 159-192

[25] N. Ohler, A.T. Bell, *J. Catal*. 231(1) (2005) 115-130

[26] Y. Cui, Y. Xia, J. Zhao, L. Li, T. Fu, N. Xue, L. Peng, X. Guo, W. Ding, *Appl. Catal. A: Gen*. 482 (2014) 179-188

[27] Y. Zhang, G. Zhang, Y. Zhao, X. Li, Y. Sun, Y. Xu, *Int. J. Hydrogen Energy* 37 (2012) 6363-6371

[28] M. Jiang, B. Wang, Y. Yao, Z. Li, X. Ma, S. Qin, Q. Sun, *Appl. Surf. Sci*. 285P (2013) 267–277

[29] M. M. Mohamed, S.M.A. Katib, *Appl. Catal. A: Gen*. 287 (2005) 236–243

[30] D. Andreeva, P. Petrova, L. Ilieva, J.W. Sobczak, M.V. Abrashev, *Appl. Catal. B: Env*. 77 (2008) 364–372

[31] G. Mitran, O. D. Pavel, *Reac Kinet Mech Cat* 114 (2015) 197–209

[32] C. Lin, M. Yu, Z. Cheng, C. Zhang, Q. Meng, J. Lin, *Inorg. Chem*. 47 (2008) 49-55

[33] M.A.F. Monteiro, H.F. Brito, M.C.F.C.M. Felinto, G.E.S. Brito, E.E.S. Teotonio, F.M. Vichi, R. Stefani, *Micropor. Mesopor. Mater.* 108 (2008) 237–246

[34] J. Vakros, C. Papadopoulou, G. A. Voyiatzis, A. Lycourghiotis, C. Kordulis, *Catal. Today* 127 (2007) 85–91

[35] V. S. Escribano, J.M. G.Amores,E. F.Lopez, C. Martinez,G. Busca, C. Resini, *Mat. Chem. Phys*. 114 (2009) 848–853

[36] E.V. Kondratenkoa, Y. Sakamoto, K. Okumura, H. Shinjoh, *Catal. Today* 164 (2011) 46–51

[37] T. Tsoncheva, R. Ivanova, J. Henych, M. Dimitrov, M. Kormunda, D. Kovacheva, N. Scotti, V. Dal Santo, V. Stengl, *Appl. Catal. A: Gen*. 502 (2015) 418–432

[38] L. Wang, W.K. Hall, *J. Catal*. 77 (1982) 232-241

[39] M.C. Abello, M.F. Gomez, M. Casella, O.A. Ferretti, M.A. Bañares, J.L.G. Fierro, *Appl. Catal. A: Gen*. 251 (2003) 435–447

[40] K. C. Mouli, S. Mohanty, Y. Hu, A. Dalai, J. Adjaye, *Catal. Today* 207 (2013) 133– 144

[41] N. Al-Yassir, R. Le Van Mao, *Appl. Catal. A: Gen. 332* (2007) 273–288

[42] R. Alcala, M. Mavrikakis, J.A. Dumesic, *J. Catal*. 218 (2003) 178-190

[41] X.D. Wang, S.R. Li, H. Wang, B. Liu, X.B. Ma, *Energ Fuel* 22 (2008) 4285-4291

[43] Y.C. Lin, *Int. J. Hydrogen Energy* 38 (2013) 2678-2700

[44] S. Ramesh, E. H. Yang, J.S. Jung, D. Ju Moon, *Int. J Hydrogen Energy* 40 (2015) 11428-11435

[45] C. Dave, K. Pant, *Renew. Energy* 36 (2011) 3195-3202

[46] G. Mitran, O.D. Pavel, M. Florea, D. Mieritz, D. K. Seo, *Catal. Commun*. 77 (2016) 83-88

[47] S. Adhikari, S. Fernando, A. Haryanto, *Catal. Today* 129 (2007) 355–364

[48] W.S. Dong, H.S. Roh, K.W. Jun, S.E. Park ,Y.S. Oh, *Appl. Catal. A: Gen* 226 (2002) 63-72

[49] L.F. Bobadilla, A. Penkova, A. Álvarez, M.I. Domínguez, F. Romero-Sarria, M.A. Centeno, J.A. Odriozola, *Appl. Catal. A: Gen*. 492 (2015) 38–47